Robotica: (2021) volume 39, pp. 686–698. © The Author(s), 2020. Published by Cambridge University Press.
doi:10.1017/S0263574720000661

A Quadruped Soft Robot for Climbing Parallel Rods

Nana Zhu**, Hongbin Zang**,*, Bing Liao, Huimin Qi, Zheng Yang, Mingyang Chen, Xin Lang and Yunjie Wang

School of Manufacturing Science and Engineering, Key Laboratory of Testing Technology for Manufacturing Process, Ministry of Education, Southwest University of Science and Technology, Mianyang 621010, China

(Accepted June 19, 2020. First published online: July 16, 2020)

SUMMARY
Soft robots can perform effectively inspecting than rigid robots in some special environments such as nuclear pipelines and high-voltage cables. This article presents a versatile quadruped soft rod-climbing robot (SR-CR) that consists of four bending actuators and a telescopic actuator. The bending actuator is composed of flexible bellows with multiple folding air chambers, elastic telescopic layer (ETL), and strain-limiting layer (SLL). The telescopic actuator provides the energy for the robot to climb forward. The SR-CR is activated by a control strategy that alternates the body deformation and feet pneumatic clenched for stable climbing. The robot can climb rods at 90°, with the maximum speed of up to 2.33 mm/s (0.018 body length/s). At 0.83 HZ, the maximum moving speed of the robot in climbing horizontally parallel rods can reach 18.43 mm/s. In addition, the SR-CR can also achieve multiple impressive functions, including turning around a corner at a rate of 7 mm/s (0.054 body length/s), carrying a payload of 3.7 times its self-weight on horizontal rods at a speed of 9 mm/s (0.069 body length/s).

KEYWORDS: Climbing robot; Bending actuator; Telescopic actuator; Flexible bellows; Locomotion.

1. Introduction

Climbing soft robots have attracted tremendous interest of researchers because of their potential applications in intelligent surveillance, inspection, and maintenance.[1–3] Over the last few decades, a great number of climbing robots have been developed, and various types of experimental prototypes and products have been proposed. With respect to the locomotive mechanism, climbing robots can be divided into six categories: legs, wheels, vacuum suction cups, magnetic hand, adhesive materials, and grippers.[4] However, the applications of rigid climbing robots are limited due to their inflexible actuators. Moreover, their movement also mostly depends on rigid actuators such as electric motors and electromagnetic, so these robots are usually heavy, poor environmental adaptability, expensive manufacturing costs, not safety and reliability, and their bodies are inflexible as organisms.[5–9] Although researchers have long been proposing some methods to address mainly problems such as manipulation accuracy and positioning error, climbing robots still not avoid to integrate complex algorithms and sensors.[10] For example, snake robots can climb over a flange on a pipe, but the robot's design is too complex and motion is not flexible because it is formed by connecting 10 segments with different motions.[11]

* Corresponding author. E-mails: zanghongbin@swust.edu.cn, zanghongb@163.com
** These authors contributed equally to this work.

https://doi.org/10.1017/S0263574720000661 Published online by Cambridge University Press

The rise of soft robots has brought new solutions to the above problems because they consist of deformable soft materials, which can meet the high demand of compliance, durability, and elasticity.[12–15] Hence, soft robots have been developed to adapt to special environments according to their excellent characteristics.[16–21] Moreover, motor-rope,[22] pneumatic,[16,18,19,21,23,24] hydraulic,[25] shape memory alloy,[26] dielectric elastomer,[27–35] chemical reaction,[20] light,[36,37] or magnetic field[38] provide driving force for the movement of soft robots. Their work modes mainly are crawling,[39–46] climbing,[16,23,24,27,47,48] and so on. Different combinations of driven methods and movement modes benefit the application of soft robots. Therefore, extensive work has been devoted to developing various soft crawling and climbing robots due to their unique advantages work on special environments. Verma et al.[16] built the soft tube-climbing robot using buckling pneumatic actuators by powered vacuum, which can navigate through a tube and remove obstacles from tubes to perform a clearing function. Jiao et al.[23] developed a vacuum-powered soft pipe-climbing robot that could achieve linear and twisting movements by employing different combinations of vacuum-powered soft pneumatic actuators. Although these soft robots are capable of moving inside of tube, their operating mechanism is not well suited for climbing rods. Recently, Tanget al.[24] designed a load-carrying amphibious climbing soft robot via combining the switchable adhesion actuator achieved by negative pressure with a soft bending actuator, which could be applied to multifunctionality in window cleaning and underwater inspection under harsh environment. Gu et al.[27] achieved a soft wall-climbing robot based on muscle-like actuators. It is enabled by a control strategy that synchronizes the body deformation and feet electroadhesion for stable climbing. Qin et al.[46] reported a versatile soft crawling robot capable of rapid and effective locomotion. The robot mainly consists of two vacuum-actuated spring actuators and two electrostatic actuators, which can achieve two basic modes of locomotion: linear motion and turning. Kanada et al.[47] introduce a robot called longitudinally extensible continuum robot, which shows successful locomotion transition from one surface to another at angles between 0° and 180°. Moreover, these soft climbing robots can hardly climb on wall with large curved surface, or rods with small diameter, although they can achieve climbing locomotion on vertical or inclined smooth surfaces.

The above research work is very valuable and innovative, but it is difficult to meet the increasing complex problems of bending rod, variable diameter, and obstacle climbing in actual applications. Therefore, the research and development of new rod-climbing technology is an important direction in the field of rod-climbing robot. However, to our best knowledge, the report on soft robot for climbing robot is rare till today. The main challenges of soft rod-climbing robot (SR-CR) design are (i) soft materials capable of adapting to the surface with large curvature generate sufficient grip force to support robot's body weight and (ii) soft actuators can generate great propulsion to improve locomotion capability when the one end of robot is anchored.

In this paper, we propose a versatile quadruped SR-CR that consists of four bending actuators and a telescopic actuator. The SR-CR can climb steadily on parallel rods owing to large grasping force of bending actuators, and the maximum 1.5 times elongation of telescopic actuator. Then, a theoretical model is developed to interpret bend and linear motion of bending actuator and telescopic actuator with air pressure, respectively. A control strategy implemented by Arduino is used to achieve fast locomotion of the robots. Furthermore, we demonstrate that the proposed robots can perform climbing locomotion with a maximum speed of 18.43 mm/s, turning down a corner with a speed of 7 mm/s, climbing on parallel rods with different diameter, and carrying a payload or camera to record video. This work can largely push the soft robot capabilities and multifunctionality in special environment such as nuclear pipelines and parallel rods high-voltage cables.

2. Design and Control of SR-CR

2.1. SR-CR design

Given 400 kPa, the two sides of the bending actuator have different stresses, which causes the actuators can deform and grip rods. Depending upon this principle, we designed and fabricated an SR-CR. As shown in Fig. 1(a), the device is composed of two slender rods, four bending actuators, and a telescopic actuator. The middle part is the telescopic actuator. The parts at both ends are bending actuators. The robot is motivated to climb up the rods by controlling the inflation and deflation of

https://doi.org/10.1017/S0263574720000661 Published online by Cambridge University Press

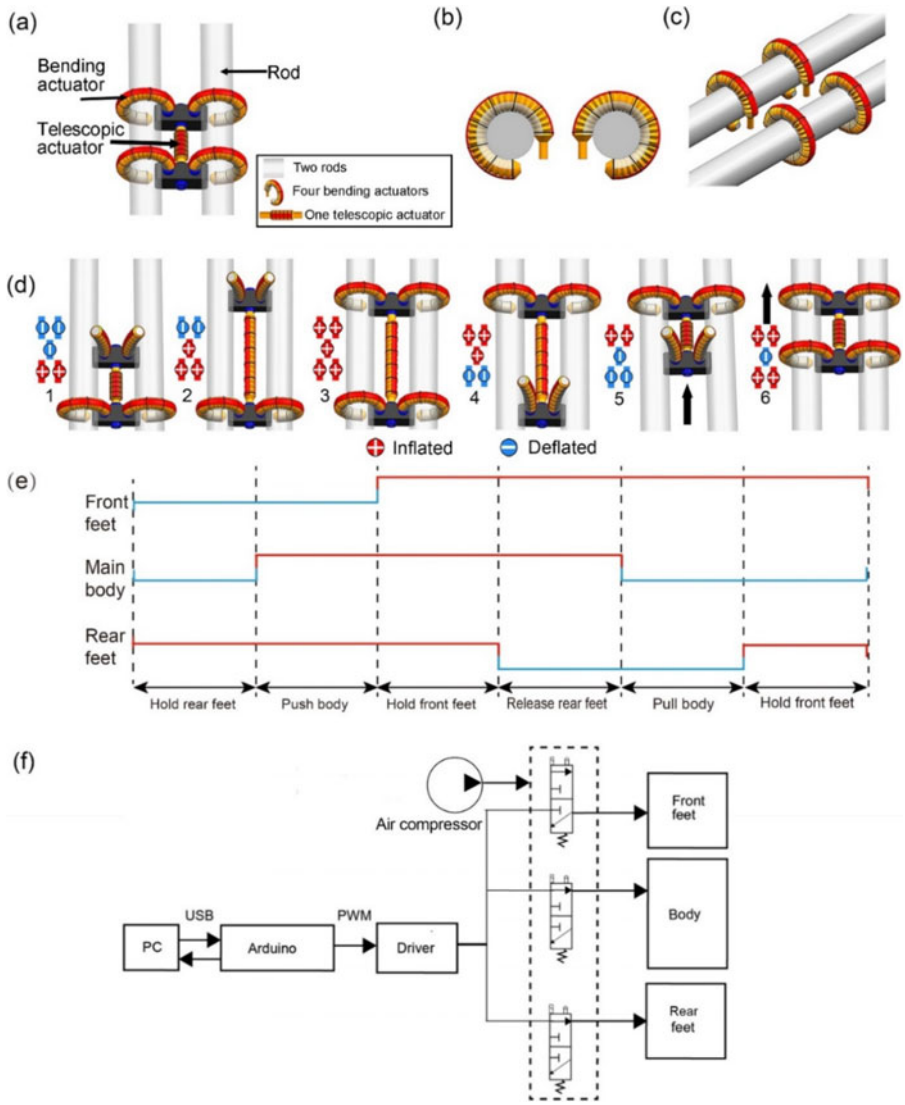


Fig. 1. Schematics of a rod-climbing robot powered with telescopic actuator. (a) The schematic diagram of robot climbing on the parallel rods. (b) Front view of the actuator which is clenching rods. (c) The side view of bending actuator which is gripping rods. (d) Motion sequence diagram of SR-CR, where blue portions indicate the pressured actuator and red portions indicate the unpressured actuator. (e) Sequence of pressure used in each pneumatic control channel for climbing, where the blue line indicates the state of inflation, and the red line indicates the state of deflation. (f) Control system of the SR-CR.

these three parts independently. Figure 1(b) and (c) shows the pressured state of the bending actuators. The design strategy of robot motion is shown in Fig. 1(d). Blue portions and red portions indicate the state of unpressured and pressured, respectively. Climbing is achieved by periodic actuation of six steps described as follows. In the first step, the rear feet is driven to grip the rods, and the body and front feet remain in the unpressured state. The second step is to drive the body part of the robot, and the front feet still remain in the unpressured state. In the third step, the front feet is driven for clenching the rods, and the body and rear feet remain in the pressured state. In the fourth step, the pressure of the rear feet is released to loosen rods, and the front feet and body are kept as the pressured state. The fifth step, the air pressure of the body is released, the front feet remains in the actuated state and the rear feet remain in the relaxed state. In the sixth step, the rear feet clench rods, the front feet maintains the driven state, and body maintains the relaxed state. Figure 1(e) clearly presents the air pressure sequence of each part of SR-CR. Figure 1(f) presents the control system of

https://doi.org/10.1017/S0263574720000661 Published online by Cambridge University Press

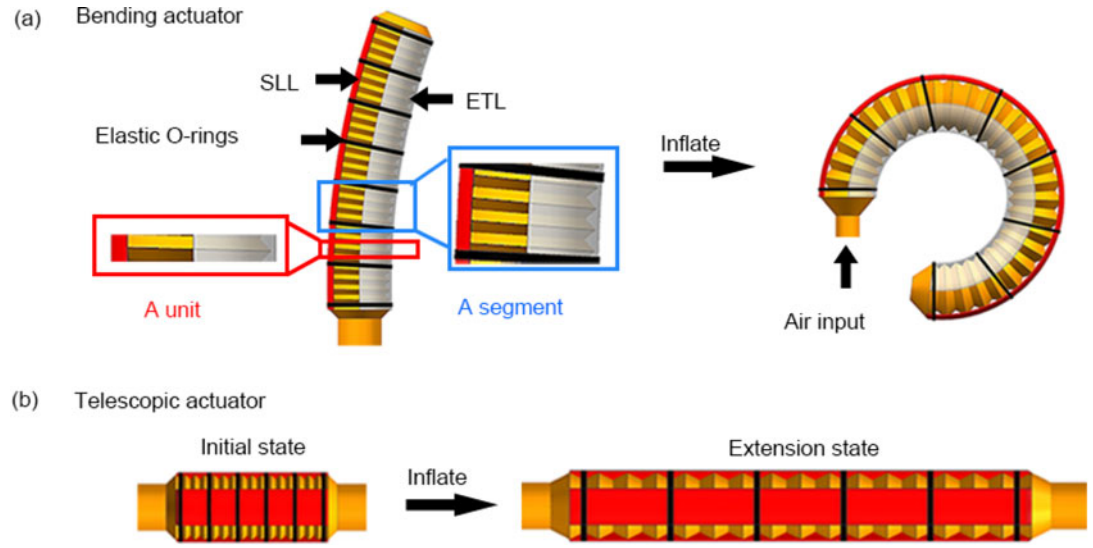


Fig. 2. Deformation motion of two actuators. (a) The actuator deforms with the increase of air pressure. (b) Schematic diagram of the telescopic actuator during depressurization and pressurization.

SR-CR. A personal computer hosting the user interface is connected to an Arduino Mega 2560 using USB and sends commands for specific motions. The pneumatic inputs are connected to the pressure source via valves. The Arduino generates a pulse-width modulation signal based on the command and supplies voltages to two-position three-way solenoid valve (24 V Direct Current Ou Si Tuo) via drivers (L298N).

2.2. Actuators design

The SR-CR is composed of four bending actuators and a telescopic actuator. Bending actuator used as the feet of the robot is the essential part of SR-CR, which has seven segments (each segment has four folding units). Bending actuator comprises flexible bellows, elastic telescopic layer (ETL), strain-limiting layer (SLL), and elastic O-rings. When the actuator is pressurized, the actuator changes from the initial state to the bending state, which is similar to an "O" shape. The bending actuator is retracted through the elastic potential energy released by ETL (Fig. 2(a) and Supplementary Movie S1). As the body part of the robot, the construction of telescopic actuator is largely the same as the previous work described in Liao et al. [48] with five segments, each of which has three folding units. The telescopic actuator consists of ETL, flexible bellows, and multiple O-rings. ETL is a ring-array structure, the array number is three, which endows the actuator with scalability when pressurized (Fig. 2(b)). Additionally, detailed basic parameters of SR-CR are shown in Table A1 (Appendix).

2.3. Design parameters

Understanding the effects of geometric variables on performance of the actuators in fabrication process is critical to adjusting input pressure range. There is a critical design parameter: the number of folding units contained in each segment of the actuators (Fig. 3). Elongation rate increases with the number of folding units in each segment and air pressure during the fabrication process of the telescopic actuator but decreases once the number of units exceeds 5 (Fig. 3(a)). The reason for the drop is that the telescopic actuator bends unexpectedly under pressure because its body is too soft. The most stable body is a five-segment telescopic actuator with three folding units per segment. Bending actuators with different number of folding units can be adapted to rods with different diameter ranges and shapes according to regulating pressure (Fig. 3(b)). We choose a 4-unit bending actuator as a prototype for subsequent experiments due to more stable curve.

https://doi.org/10.1017/S0263574720000661 Published online by Cambridge University Press

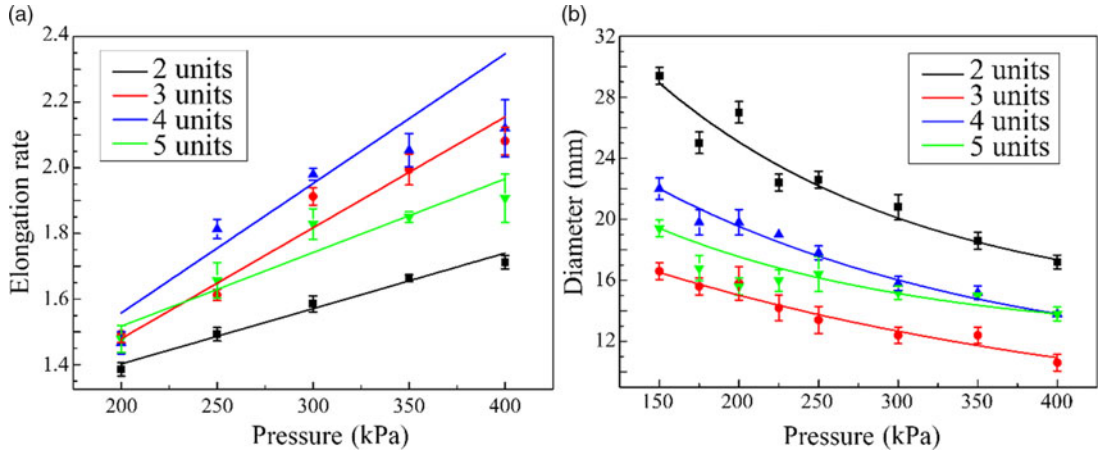


Fig. 3. The effect of actuator geometry on performance. (a) Elongation rate of the telescopic actuator with 2,3,4, and 5 units as a function of air pressure, respectively. (b) Diameter of the bending actuator with 2,3,4, and 5 units as a function of air pressure, respectively.

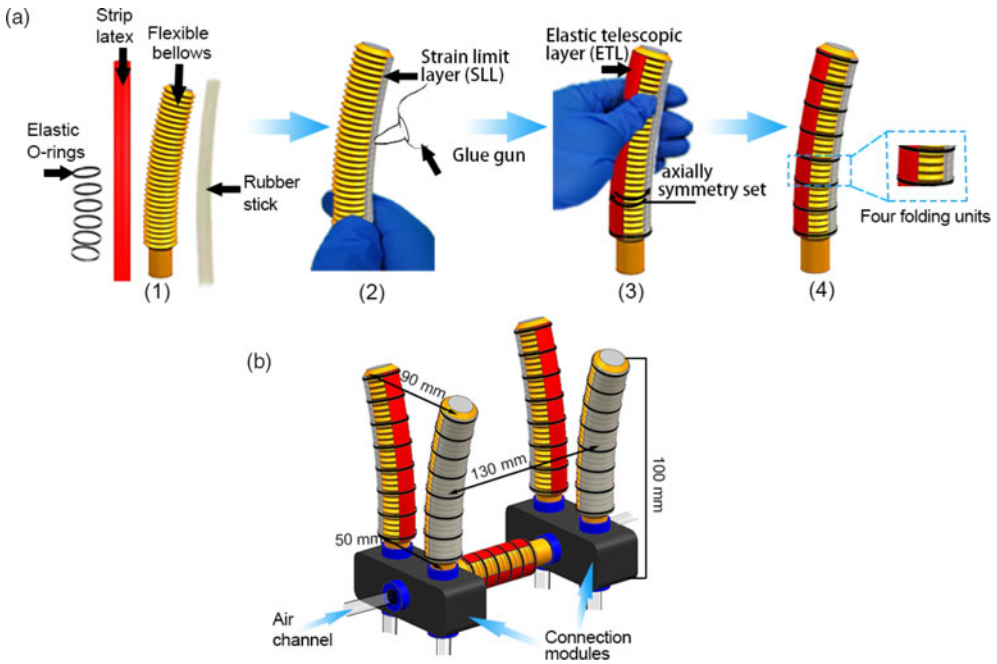


Fig. 4. The fabrication steps of the SR-CR. (a) The fabrication steps of the bending actuator. (b) Model diagram of SR-CR.

3. Materials and Methods

3.1. Fabrication method

Different from methods of modeling, pouring, and demolding, the proposed fabrication method for soft robots is simpler, more efficient, more general, and lower cost. We just use the common off-the-shelf materials. Figure 4(a) shows the fabrication process of the bending actuator, which mainly includes four steps. (1) The needed materials are prepared: flexible bellows, rubber stick, strip latex, and elastic O-rings. (2) Rubber stick is loaded into the glue gun. After the rubber stick is melt, hot melt adhesives are coated in the inner side of the flexible bellows. The advantage of hot melt adhesives is that the direction, area, and thickness of the SLL can be adjusted as required. (3) ETL is established in the direction of axial symmetry of SLL. That is the outside of the bellows. (4) ETL, flexible bellows, and SLL are fixed using elastic O-rings, and a segment is composed of four folding units. The fabrication procedures of the telescopic actuator is relatively easy, which are wrapped annularly by three ETLs [48].

https://doi.org/10.1017/S0263574720000661 Published online by Cambridge University Press

Connecting modules were casted in the 3D printed molds (Makerbase robin gen). The size is 56 mm × 20 mm × 20 mm. The drive system is oil-free air compressor (OLF-800-4). As shown in Fig. 4(b), the six two-way connectors are installed into two connection modules, which are exactly the same symmetrical arrangement. Front feet, body, and rear feet are separately connected by two connection modules, each of which actually is connected to a silicone tube. Only three pneumatic paths are needed to control the inflation and deflation of three parts (front feet, body, and rear feet) of the robot. The rods (diameter, 20 mm; length, 30 mm) used for climbing experiments are made of polyvinyl chloride material. The mass of the robot is 61 g.

3.2. Theoretical model

The bellows is strongly deformed as the increase of air pressure and it cannot return to initial state if the pressure is released. The deformation recovery of actuators is closely dependent on the restoring force of the ETL. Based on the theoretical model of Liao et al. [48], in the steady state when the telescopic actuator is deformed, the expansion force F_1 (Eq.1) obtained by the air pressure is equal to the restoring force F_2 (Eq. 2) generated by the ETL.

$$F_1 = \mathrm{PS}_1 \tag{1}$$

$$F_2 = \mathrm{k}_1\mathrm{L} \tag{2}$$

$$S_1 = \pi\left(\frac{R+r}{2}\right)^2 \tag{3}$$

$$\mathrm{L} = \frac{\pi P\left(\frac{R+r}{2}\right)^2}{k_1} \tag{4}$$

where P presents the supply pressure, k_1 presents the elastic coefficient of the ETL ($k_1 = 0.945$), k is measured by a pressure dynamometer (NK-100; Samsung, Japan), L is the deformation of the telescopic actuator, S_1 denotes the cross-sectional area of the bellows (Eq. 3), and r and R present the inner and outer radius of the bellows, respectively (Fig. 5(a)). Thus, the relationship between deformation of the telescopic actuator and the air pressure can be obtained by Eq. (4). As shown in Fig. 5(b), the previous work shows the experimental data are mostly near the theoretical model [48]. The error between the experimental data and the theoretical prediction is caused by handcrafting. At 400 kPa, the elongation rate of the telescopic actuator reaches maximum.

Similarly, based on the method that the constant curvature model is inflated and the SLL is not deformed when the bending actuator is inflated, it is concluded that the working principle of the soft actuator is the bending deformation caused by the arc length difference between the inner and outer diameters, as shown in Fig. 5(c). E denotes the outer arc length before deformation, and H denotes the outer arc length after deformation. When the actuator micro-element is bent and stabilized, the pressure F_1 (Eq. 1) generated by the inflation is equal to the restoring force F_3 (Eq. 5) generated by the ETL stretched.

$$F_3 = k_2(H - \mathrm{E}) \tag{5}$$

where k_2 denotes the elastic coefficient of the ETL ($k_2 = 0.45$), Q denotes the arc length of the ETL, and β denotes the central angle. Utilizing arc length (Eq. 6 and Eq. 7), the inner arc length, and outer arc length are calculated after the bending actuator deformed. Finally, the relationship between the deformation radius (represented by b) of the bending actuator and the air pressure can be obtained by Eq. (8).

$$Q = \beta b \tag{6}$$

$$H = \beta\,(b + r + R) \tag{7}$$

$$b = \frac{k_2 Q(r+R)}{k_2(E-Q) + \pi P\left(\frac{R+r}{2}\right)^2} \tag{8}$$

https://doi.org/10.1017/S0263574720000661 Published online by Cambridge University Press

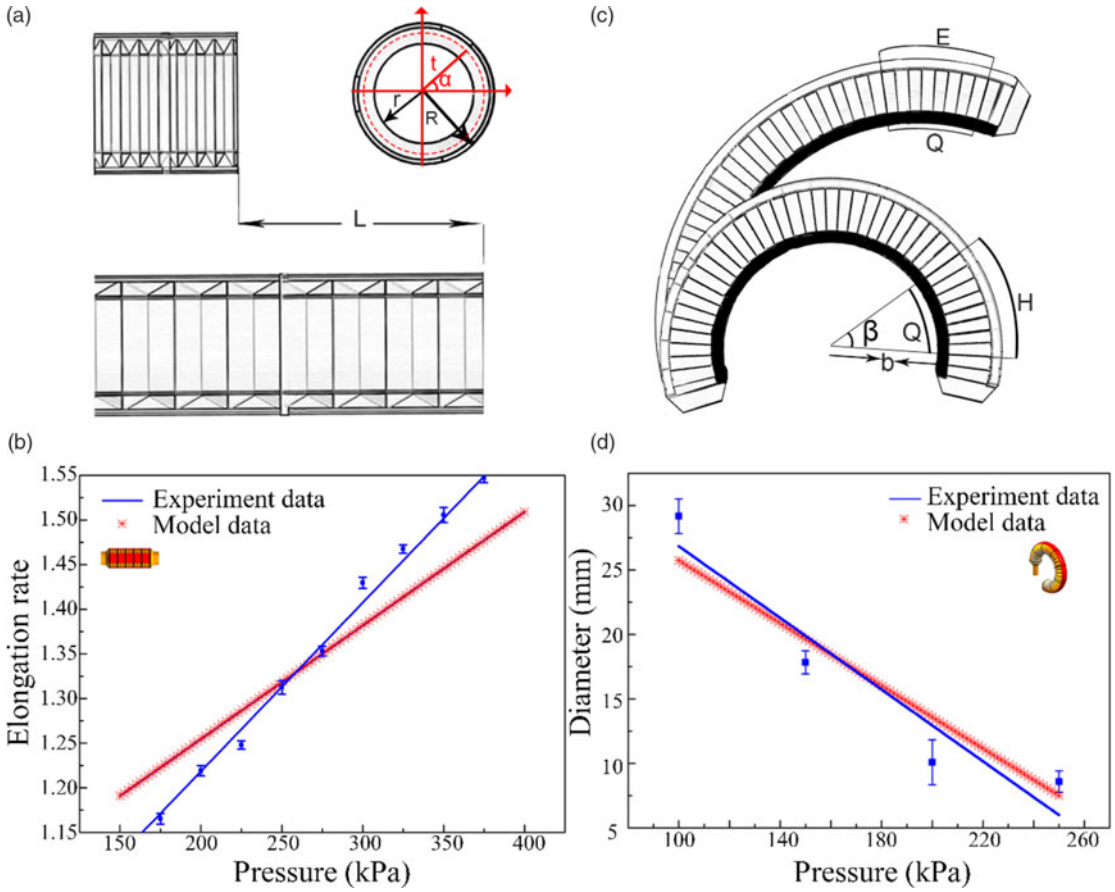


Fig. 5. Model of the actuators. (a) Model of the telescopic actuator. (b) Comparison between the theoretically predicted and tested the elongation rate of the telescopic actuator vs. supplied pressure relationships. (c) Model of the bending actuator. (d) Comparison between the theoretically predicted and tested the radius of the bending actuator vs. supplied pressure relationships.

When the bending actuator is not deformed, the inner and outer arc lengths of the respective micro-element portions are approximately equal. Therefore,

$$\mathrm{E} = \mathrm{Q} \tag{9}$$

$$\mathrm{b} = \frac{4k_2 Q}{\pi P(R+r)} \tag{10}$$

According to Eq. (9), the relationship in Eq. (8) can be simplified to Eq. (10). As shown in Fig. 5(d), it is concluded that the radius of the bending actuator is linear with the air pressure. The correctness of the proposed theory model is verified by experiments. At 250 kPa, the radius of the bending actuator reaches minimum. The deformation state of the actuator can be changed by controlling the pressure.

4. Results

Figure 6(a) and (b) show feasibility of SR-CR fabrication methods. Due to strong adhesion between SLL and flexible bellows, the bellows has a slight bending effect. As shown in Fig. 6(c), the movement process is mainly divided into six steps. The five functional units (four bending actuators and a telescopic actuator) are actuated in sequence to make the robot to climb parallel rods. Experimental results of climbing cycle of SR-CR keep a good consistence with the design strategy mentioned above (Fig. 1(d)).

https://doi.org/10.1017/S0263574720000661 Published online by Cambridge University Press

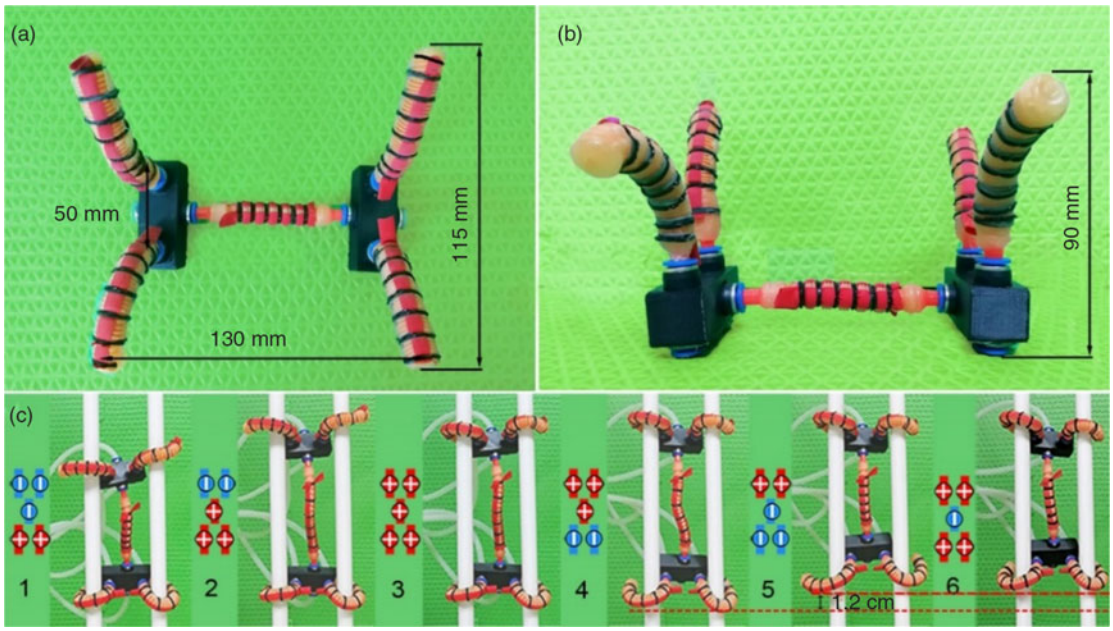


Fig. 6. The experiment of SR-CR. (a) Top view of SR-CR. (b) Side view of SR-CR. (c) One climbing cycle (each panel corresponds to the steps of the schematic in Fig. 1(d)). The rod climber moves in vertical rods at the rate of 2.33 mm/s, and distance covered over one cycle is 1.2 cm. The red areas in the image are inflated state, and the blue areas are deflated state.

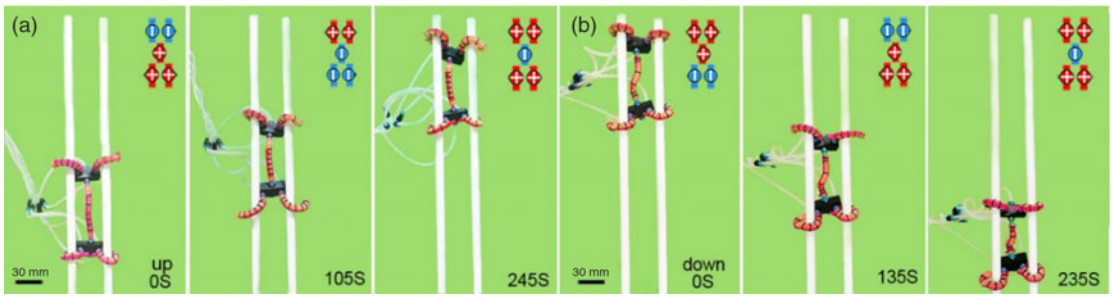


Fig. 7. Demonstration of the SR-CR climbing on the parallel rods. (a) The robot climbs upward under the challenge of gravity. (b) The robot climbs downward.

4.1. Vertical rod experiment

When the input air pressure is 400 kPa, the robot firmly clenches the slender rods. Climbing performance of the robot in vertical directions is tested (Fig. 7 and Supplementary Movie S2). The result demonstrated that the upward speed can reach about 2.33 mm/s (0.018 body length/s), and the downward speed is about 2.52 mm/s. Since the segments of the body part of the robot are composed of four units, during the climbing process of the robot, the bending curvature of the body part is relatively large and the stretching amount is reduced, resulting in the reduction of the climbing efficiency of the robot. Because the robot needs to elongate and contract against sliding forces to climb rods, the telescopic actuator plays an important role in driving of SR-CR. The extension rate of the telescopic actuators is closely related to ETL. Flexible bellows elongate driven by the airflow, and then it returns to the original position by releasing elastic potential energy stored in ETL, which can drive the robot to climb forward.

4.2. Horizontal rod experiment

The performance of SR-CR on the horizontal climbing efficiency was tested. It is found from the experimental results that climbing speed of the robot with the flexible bellows fully wrapped by ETL (Fig. 8(a)–(c) and Supplementary Movie S3) is twice that of robot with the bellows annularly

https://doi.org/10.1017/S0263574720000661 Published online by Cambridge University Press

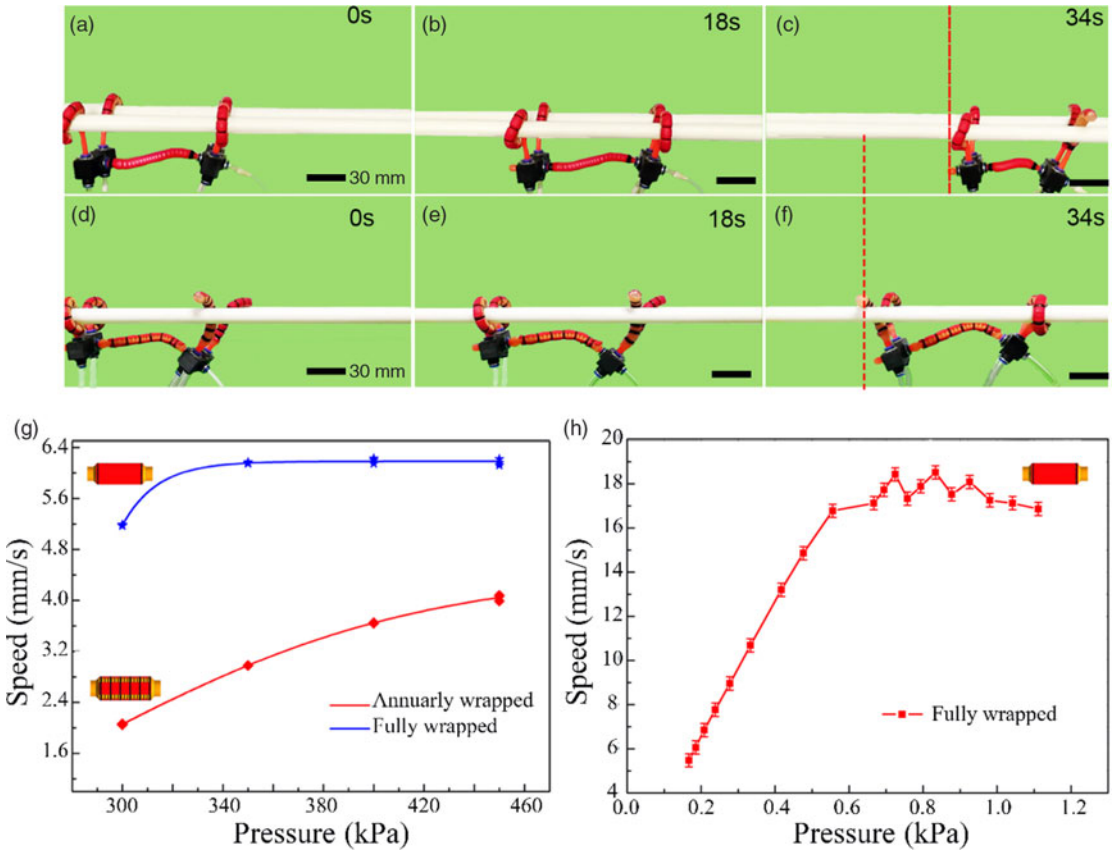


Fig. 8. Climbing results of the soft robot. (a–c) The movement of the robot in horizon direction, in which the robot body is wrapped fully with ETL. (d–f) The robot climbs on parallel rods, which body is wrapped annularly with ETL. (g) Comparison diagram of the speed of the robot with bellows annularly wrapped and fully wrapped. (h) Speed plotted as a function of 1/T on horizontal rods.

wrapped by ETL (Fig. 8(d)–(f) and Supplementary Movie S4). As shown in Fig. 8(g), the climbing speeds of the telescopic actuators with fully wrapped and annularly wrapped were compared at different pressures. The former maximum speed is 6.18 mm/s with a period of 6s (per cycle), and the latter maximum speed of is 4.05 mm/s. At 450 kPa, the climbing speed of the robot with the bellows annularly wrapped reach maximum.

4.3. Frequency experiment

Frequency is also essential to the design of a climbing robot. We applied a variable frequency adjusted by the controller from 0.17 HZ (T = 6 s) to 1.1 HZ (T = 0.9 s) at 400 kPa pressure value. It can be seen that the speed is larger with the increase of the frequency, but it starts to fluctuate from the 17 mm/s (Fig. 8(h)). It is assumed that the materials and surface roughness of the rods could affect the speed. Then, we measured the maximum speed at each cycle achieved by the robot. The maximum moving speed of the robot in climbing horizontally can reach 18.43 mm/s. The speed is averaged from at least 10 periods per frequency according to the recorded videos (Supplementary Movie S5), and the speed is 3 times higher than the measured before (Supplementary Movie S3).

4.4. Diameter of the rod

We also evaluated the effect of the different diameters of the rod (Polyvinyl chloride; diameter, 16 mm, 20 mm, 25 mm, and 32 mm, respectively) and square rod (length, 20 mm; width, 10 mm) on the performance of the robot (Fig. 9 and Supplementary Movie S6). The results show that speed of the robot achieves the maximum value when climbing on parallel rods with a diameter 25 mm.

https://doi.org/10.1017/S0263574720000661 Published online by Cambridge University Press

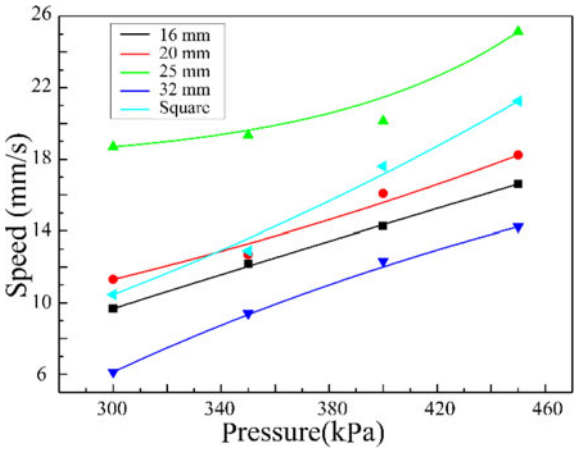


Fig. 9. The effect of the diameter of the rods and square rod on the performance of the robots.

The reason that affects the performance change is that the feet of the robot cannot strongly grasp the rods (diameter, 16 mm and 20 mm) because ring formed by the bending actuator is larger than that of the rod, resulting in unstable climbing. For current prototype size, on the other hand, the robot's speed will also be reduced if they climb over sized rods (diameter, 32 mm). The speed of climbing square rod is slightly higher than 20-diameter rod because they all have almost the same size.

5. Application of SR-CR

The potential applications include climbing vertically, climbing bending rods, equipping with cameras and climbing with load horizontally. As shown in Fig. 10(a)–(c) and Supplementary Movie S7, the robot climbs along the curved rod-shaped surfaces and turns a corner successfully with the speed of 7 mm/s.

This result indicates that the robot can navigate autonomously in case of cornering. Moreover, a small camera (weight, 37 g; length, 33 mm; width, 33 mm; height, 33 mm; model-MINI20-DA) is loaded on the robot, so that it could take videos while climbing parallel rods horizontally. As a result, the images at a certain view were recorded by camera (Fig. 10(d)–(f) and Supplementary Movie S8). Figure 10(g)–(i) and Supplementary Movie S9 show that SR-CR moves horizontally while carrying a 224-g payload. The payload is 3.7 times its own weight (mass 61 g), and the speed of climbing with load is 9 mm/s. Therefore, this kind of robot can serve well for the requirement of multimodal motion and high-load-carrying capacity in some special environments such as nuclear pipelines and parallel rods high-voltage cables.

6. Discussion

The results show that the structure of soft robot differs from that of rigid robots, which can realize the large deformation and high flexibility. The soft robot has many functions, including climbing horizontally with load and climbing bending rods. However, some aspects of the proposed soft robot should be improved, including the following points. (1) The connecting module should be designed as an empty shell or more elaborate structure. (2) Carrying larger load may be required for the SR-CR robot, which ensures the robot to carry control circuits and air equipment to complete tasks. (3) The body part of the robot is too soft. It cannot produce enough force to overcome the friction caused by the feet and the rods. Designing a better structure of the body part of the robot is our next work. For example, two plastic tubes with diameter difference can be used to design a guide mechanism installed inside the telescopic actuator to improve the extendibility of robots effectively. (4) The proposed soft robot requires external wires and the power source, which may limit its functionality especially in some practical applications. In the future, developing a fully untethered soft robot with the power source and control circuits on board is also our next work.

https://doi.org/10.1017/S0263574720000661 Published online by Cambridge University Press

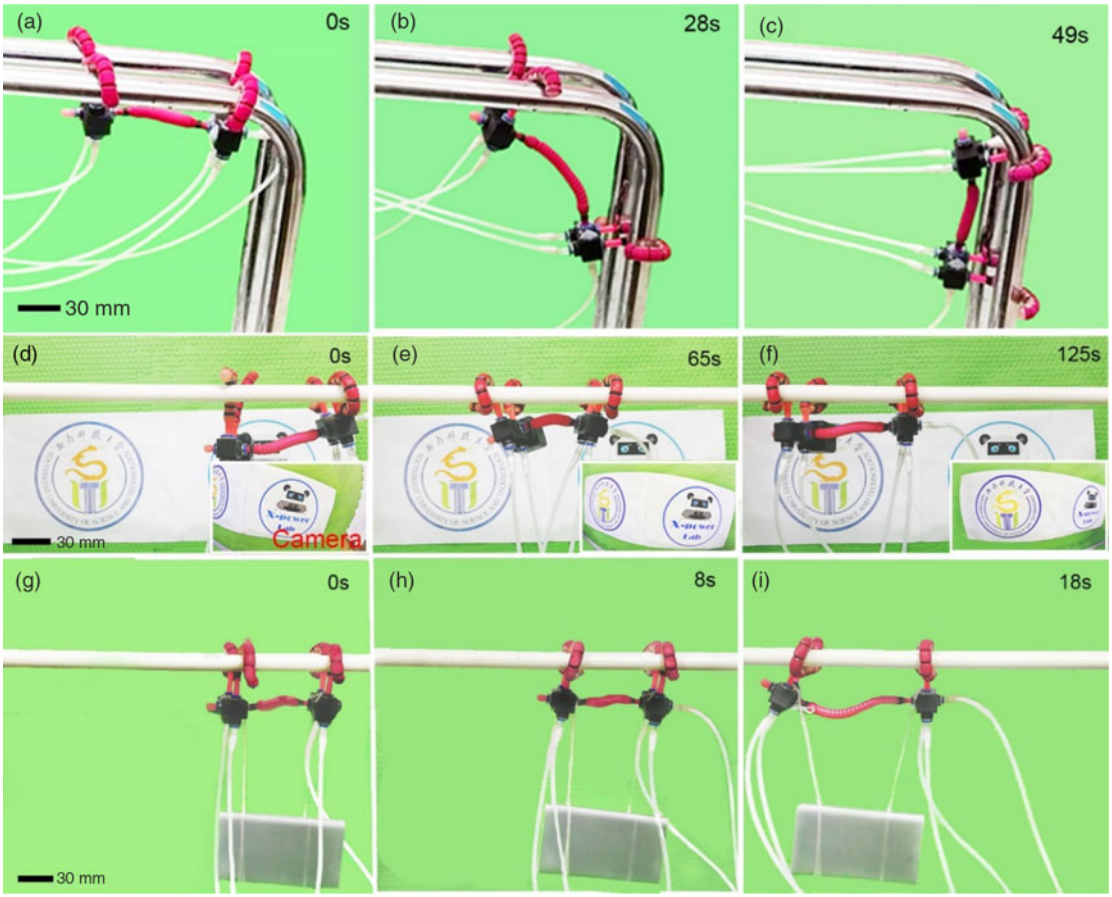


Fig. 10. The application of the SR-CR. (a–c) Still images illustrate the climbing process of the SR-CR when turning around a corner. (d–f) The SR-CR carrying camera moves horizontally and video recording process. (g–i) The rod climber moves along rods horizontally with a 224-g payload.

7. Conclusions

In this paper, a versatile quadruped SR-CR with simple structure, stable movement, and strong environmental adaptability is designed. The robot body, made of a telescopic actuator, extends with air pressure and recovers to the original state after deflation, which ensures a great deformation per actuation cycle. The robot feet, made of four bending actuators, can clench on the rod surface without slippage to improve the locomotion efficiency. Moreover, our SR-CR has three distinctive advantages. (1) The robot can withstand large strains and deformations thanks to its soft actuators. (2) The control system of the soft robot is very simple (with merely air pressure). (3) The soft robot has multimodal locomotion, such as climbing on vertical and horizontal rods, turning around a corner, climbing different diameter rods, and carrying a payload.

Acknowledgments

This work was supported by Postgraduate Innovation Fund Project by Southwest University of Science and Technology (Grant No. 19ycx0120), The Doctoral Research Fund of Southwest University of Science and Technology in China (Grant No. 19zx7166), and Research Foundation of Southwest University of Science and Technology (Grant No. 18zx7162).

Author Disclosure Statement

No competing financial interests exist.

https://doi.org/10.1017/S0263574720000661 Published online by Cambridge University Press

Supplementary material

To view supplementary material for this article, please visit https://doi.org/10.1017/S0263574720000661.

References

1. F. Xu, J. L. Hu and G. Jiang, "The obstacle-negotiation capability of rod-climbing robots and the improved mechanism design," *J. Mech. Sci. Technol*. **29**(7), 2975–2986 (2015).
2. R. Chen, R. Liu, J. Chen and J. Zhang, "A gecko inspired wall-climbing robot based on electrostatic adhesion mechanism," **In**: *IEEE International Conference on Robotics & Biomimetics IEEE*, Shenzhen, China (2013) pp. 396–401.
3. T. L. Lam and Y. Xu, "A flexible tree climbing robot: Treebot-design and implementation," In: *IEEE 300 International Conference on Robotics and Automation*, Shanghai, China. (2011) pp. 5849–5854.
4. A. Sadeghi, H. Moradi and M. Nili Ahmadabadi, "Analysis, simulation, and implementation of a human-inspired pole climbing robot," *Robotica.* **30**(2), 279–287 (2012).
5. M. Spenko, G. C. Haynes, J. A. Saunders, M. R. Cutkosky, A. A. Rizzi, R. J. Full and D. E. Koditschek, "Biologically inspired climbing with a hexapedal robot," *J. Field Robot*. **25**(4–5), 223–242 (2008).
6. F. Xu, X. Wang and G. Jiang, "Design and analysis of a wall-climbing robot based on a mechanism utilizing hook-like claws," *Int. J. Adv. Robot. Syst.* **261**(9), 1–12 (2012).
7. F. Tâche, W. Fischer, G. Caprari, R. Siegwart, R. Moser and F. Mondada, "Magnebike: A magnetic wheeled robot with high mobility for inspecting special-shaped structures," *J. Field Robot.* **26**, 453–476 (2009).
8. G. Lee, K. Seo, S. Lee, J. Park, H. Kim, J. Kim and T. Seo, "Compliant track-wheeled climbing robot with transitioning ability and high-payload capacity," **In:** *IEEE International Conference on Robotics and Biomimetics*, Karon Beach, Phuket, Thailand (2011) pp. 2020–2024.
9. H. Zhang, J. Zhang, G. Zong, W. Wang and R. Liu, "Sky Cleaner 3: A real pneumatic climbing robot for glass-wall cleaning," *IEEE Robot. Autom. Mag*. **13**(1), 32–41 (2006).
10. Mahmoud Tavakoli, Lino Marques and Aníbal T. de Almeida, "A low-cost approach for self-calibration of climbing robots," *Robotica*. **29**(1), 23–34 (2011).
11. T. Takemori, M. Tanaka and F. Matsuno, "Gait design for a snake robot by connecting curve segments and experimental demonstration," *IEEE Trans. Robot*. **34**(5), 1384–1391 (2018).
12. H. Zang, B. Liao, X. Lang, Z. Zhao, W. Yuan and X. Feng, "Bionic torus as a self-adaptive soft grasper in robots," *Appl. Phys. Lett.* **116**(2), 023701-1–023701-3 (2019).
13. D. Rus and M. T. Tolley, "Design, fabrication and control of soft robots," *Nature* **521**(7553), 467–475 (2015).
14. C. Majidi, "Soft robotics: A perspective—Current trends and prospects for the future," *Soft Robot*. **1**(1), 5–11 (2014).
15. C. Laschi, B. Mazzolai and M. Cianchetti, "Soft robotics: Technologies and systems pushing the boundaries of robot abilities," *Sci. Robot*. **1**(1), 3690 (2016).
16. M. S. Verma, A. Ainla, D. Yang, D. V. Harburg and G. M. Whitesides, "A soft tube-climbing robot," *Soft Robot.* **5**(2), 133–137 (2018).
17. X. T. Tang, K. Li and Y. X. Liu, "A soft crawling robot driven by single twisted and coiled actuator," *Sensor. Actuat. A Phys.* **291**(1), 80–86 (2019).
18. Y. Shapiro, A. Wolf and K. Gabor, "Bi-bellows: Pneumatic bending actuator," *Sensor. Actuat. A Phys.* **167**(2), 484–494 (2011).
19. M. T. Tolley, R. F. Shepherd, B. Mosadegh, K. C. Galloway, M. Wehner, M. Karpelson, R. J. Wood and G. M. Whitesides, "A resilient, untethered soft robot," *Soft Robot*. **1**(3), 213–223 (2014).
20. M. Wehner, R. L. Truby, D. J. Fitzgerald, B. Mosadegh, G. M. Whitesides, J. A. Lewis and R. J. Wood, "An integrated design and fabrication strategy for entirely soft, autonomous robots," *Nature*. **536**(7671), 451–455 (2016).
21. T. Y. Wang, L. S. Ge and G. Y. Gu, "Programmable design of soft pneu-net actuators with oblique chambers can generate coupled bending and twisting motions," *Sensors Actuat. A Phys.* **271**, 131–138 (2018).
22. C. Laschi, M. Cianchetti, B. Mazzolai, L. Margheri, M. Follador and P Dario, "Soft robot arm inspired by the octopus," *Adv. Robot*. **26**(7), 709–727 (2012).
23. Z. Jiao, C. Ji, J. Zou, H. Yang and M. Pan, "Vacuum-powered soft pneumatic twisting actuators to empower new capabilities for soft robots," *Adv. Mater. Technol*. **4**(1), 1800429 (2018).
24. Y. Tang, Q. Zhang, G. Lin and J. Yin, "Switchable adhesion actuator for amphibious climbing soft robot," *Soft Robot*. **5**(5), 592–600 (2018).
25. H. Yuk, S. Lin, C. Ma, M. Takaffoli, N. X. Fang and X. Zhao, "Hydraulic hydrogel actuators and robots optically and sonically camouflaged in water," *Nat. Commun*. **8**(1), 14230 (2017).
26. M. Munadi, M. Ariyanto, J. D. Setiawan and M. F. A. Ayubi, "Development of a low-cost quadrupedal starfish soft robot," **In:** *IEEE 5th International Conference on Information Technology, Computer, and Electrical Engineering (ICITACEE)*, (2018) pp. 225–229.
27. G. Gu, J. Zou, R. Zhao, X. Zhao and X. Zhu, "Soft wall-climbing robots," *Sci. Robot.* **3**, eaat2874 (2018)
28. J. Li, L. Liu, Y. Liu and J. Leng, "Dielectric elastomer spring-roll bending actuators: Applications in soft robotics and design," *Soft Robot*. **6**(1), 69–81 (2019).
29. H. Prahlad, R. Pelrine, S. Stanford, J. Marlow and R. Kornbluh, "Electroadhesive robots-Wall climbing robots enabled by a novel, robust, and electrically controllable adhesion technology," **In:** *IEEE International Conference on Robotics and Automation*, Pasadena, CA, USA (2008) pp. 3028–3033.

https://doi.org/10.1017/S0263574720000661 Published online by Cambridge University Press

30. A. Yamamoto, T. Nakashima and T. Higuchi, "Wall climbing mechanisms using electrostatic attraction generated by flexible electrodes," **In:** *IEEE International Symposium on Micro-Nano Mechatronics and Human Science*, Nagoya, Japan (2007) pp. 389–394.
31. S. Kalouche, N. Wiltsie, H.-J. Su and A. Parness, "Inchworm style gecko adhesive climbing robot," **In**: *IEEE/RSJ International Conference on Intelligent Robots and Systems* (2014), pp. 2319–2324.
32. O. Unver and M. Sitti, "Flat dry elastomer adhesives as attachment materials for climbing robots," *IEEE Trans. Robot*. **26**(1), 131–141 (2010)
33. J. Krahn, Y. Liu, A. Sadeghi and C. Menon, "A rear feetless timing belt climbing platform utilizing dry adhesives with mushroom caps," *Smart Mater. Struct*. **20**(11), 115021 (2011)
34. H. Wang, A. Yamamoto and T. Higuchi, "A crawler climbing robot integrating electroadhesion and electrostatic actuation," *Int. J. Adv. Robot. Syst*. **11**(12), 191 (2014)
35. H. Wang and A. Yamamoto, "A thin electroadhesive inchworm climbing robot driven by an electrostatic film actuator for inspection in a narrow gap," In: *IEEE International Symposium on Safety, Security, and Rescue Robotics (SSRR)*, Linkoping, Sweden (2013) pp. 1–6.
36. M. Rogóz, H. Zeng, C. Xuan, D. S. Wiersma and P. Wasylczyk, "Light-driven soft robot mimics caterpillar locomotion in natural scale," *Adv. Opt. Mater.* **4**(11), 1902–1902 (2016).
37. A. Chihyung, L. Kai and C. Shengqiang, "Light or thermally powered autonomous rolling of an elastomer rod," *ACS Applied Materials & Interfaces*. **10**(30), 25689–25696 (2018).
38. H. Lu, M. Zhang, Y. Yang, Q. Huang, T. Fukuda, Z. Wang and Y. Shen, "A bioinspired multilegged soft millirobot that functions in both dry and wet conditions," *Nature*. **9**(1), 3944 (2018).
39. H. Lin, G. G. Leisk and B. Trimmer, "GoQBot: A caterpillar-inspired soft-bodied rolling robot," *Bioinspir. Biomim.* **6**(2), 026007 (2011).
40. S. Seok, C. D. Onal, R. J. Wood, D. Rus and S. Kim, "Peristaltic locomotion with antagonistic actuators in soft robotics," **In**: *2010 IEEE International Conference on Robotics and Automation* (Anchorage, Alaska, 2010) pp. 1228–1233.
41. M. P. Nemitz, P. Mihaylov, T. W. Barraclough, D. Ross and A. A. Stokes, "Using voice coils to actuate modular soft robots: Wormbot, an example," *Soft Robot.* **3**(4), 198–204 (2016).
42. K. M. Shaw, H. J. Chiel and R. D. Quinn, "Efficient worm-like locomotion: Slip and control of soft-bodied peristaltic robots," *Bioinspir. Biomim*. **3**(4), 035003 (2013).
43. A. Boxerbaum, A. Horchler, K. Shaw, H. Chiel and R. Quinn, "Worms, waves and robots," **In:** *IEEE International Conference on Robotics and Automation(ICRA)*, Saint Paul, MN, USA (2012) pp. 3537–3538.
44. A. Boxerbaum, K. M. Shaw, H. J. Chiel and R. D. Quinn, "Continuous wave peristaltic motion in a robot," *Int. J. Robot. Res.* **31**(3), 302–318 (2012).
45. A. Rafsanjani, Y. Zhang, B. Liu, S. M. Rubinstein and K. Bertold, "Kirigami skins make a simple soft actuator crawl," *Sci. Robot.* **3**(15), aar7555 (2018).
46. L. Qin, X. Liang, H. Huang, C. K. Chui, R. C.-H. Yeow and J. Zhu, "A versatile soft crawling robot with rapid locomotion," *Soft Robot*. **6**(4), 455–467 (2019).
47. A. Kanada, F. Giardina, T. Howison, T. Mashimo and F. Iida, "Reachability improvement of a climbing robot based on large deformations induced by tri-tube soft actuators," *Soft Robot*. **6**(4), 483–494 (2019).
48. B. Liao, H. Zang, M. Chen, Y. Wang, X. Lang, N. Zhu, Z. Yang and Y. Yi, "Soft rod-climbing robot inspired by winding locomotion of snake," *Soft Robot*. Ahead of print (2020). DOI: 10.1089/soro.2019.0070

Table AI. Basic parameters of SR-CR.

Properties	Value	Unit
Size (L×W×H)	130 × 50 × 90	(mm)
Total mass of robot	61	(g)
Bending actuators (×4)	4	(g)
Bending actuator (D × H)	14×70	(mm)
Telescopic actuator	3	(g)
Telescopic actuator (D×H)	14×40	(mm)
Connecting device (×2)	21	(g)
Strain-limiting layer (T)	2	mm
Strain-limiting layer (W)	9	mm
Elastic telescopic layer (T)	1.6	mm
Elastic telescopic layer (W)	17	mm
Segment (H)	5.6	mm
Elastic O-ring (H)	0.1	mm

D, diameter; H, height; L, length; T, thickness; W, width.

https://doi.org/10.1017/S0263574720000661 Published online by Cambridge University Press